Ultrasound in Med. & Biol., Vol. 32, No. 11, pp. 1763–1770, 2006

0301-5629/06/$–see front matter

ELSEVIER

doi:10.1016/j.ultrasmedbio.2006.06.012

● *Original Contribution*

LESIONS OF ULTRASOUND-INDUCED LUNG HEMORRHAGE ARE NOT CONSISTENT WITH THERMAL INJURY

JAMES F. ZACHARY,*† JAMES P. BLUE, JR.,‡ RITA J. MILLER,‡ BRIAN J. RICCONI,§ J. GARY EDEN,§ and WILLIAM D. O'BRIEN, JR.†‡

*Department of Pathobiology, College of Veterinary Medicine; †Department of Bioengineering, College of Engineering; ‡Bioacoustics Research Laboratory, Department of Electrical and Computer Engineering; and §Laboratory for Optical Physics and Engineering, Department of Electrical and Computer Engineering, University of Illinois at Urbana-Champaign, Urbana, IL, USA

(*Received* 30 *January* 2006, *revised* 1 *June* 2006, *in final form* 8 *June* 2006)

Abstract—Thermal injury, a potential mechanism of ultrasound-induced lung hemorrhage, was studied by comparing lesions induced by an infrared laser (a tissue-heating source) with those induced by pulsed ultrasound. A 600-mW continuous-wave CO_2 laser (wavelength ~10.6 μm) was focused (680-μm beamwidth) on the surface of the lungs of rats for a duration between 10 to 40 s; ultrasound beamwidths were between 310 and 930 μm. After exposure, lungs were examined grossly and then processed for microscopic evaluation. Grossly, lesions induced by laser were somewhat similar to those induced by ultrasound; however, microscopically, they were dissimilar. Grossly, lesions were oval, red to dark red and extended into subjacent tissue to form a cone. The surface was elevated, but the center of the laser-induced lesions was often depressed. Microscopically, the laser-induced injury consisted of coagulation of tissue, cells and fluids, whereas injury induced by ultrasound consisted solely of alveolar hemorrhage. These results suggest that ultrasound-induced lung injury is most likely not caused by a thermal mechanism. (E-mail: zacharyj@uiuc.edu) © **2006 World Federation for Ultrasound in Medicine & Biology.**

Key Words: **Animal model, Laser injury, Lung, Pathology, Pulmonary hemorrhage, Pulsed ultrasound, Rat, Thermal injury, Ultrasound.**

INTRODUCTION

Based on the study by Hartman et al. (1992), the traditionalist view (also supported by the American Institute of Ultrasound in Medicine (2000a, 2000c)), has been that ultrasound-induced lung hemorrhage was not caused by heating. In the Hartman study, mouse lung was exposed to continuous-wave unfocused ultrasound (1.2-cm diameter 4.2-MHz source with a 3.9-mm –6-dB beamwidth). A thermocouple, used to measure temperature changes of the lung, showed approximately a 1-degree (C) rise in temperature (incident temporal-average intensity of 1 W/cm^2). It was concluded that: (1) lung was not selectively heated, (2) lung had an efficient mechanism for dissipating heat and (3) ultrasound-induced lung hemorrhage was not caused by heating.

Mechanistically, these findings suggested that ultrasound-induced lung hemorrhage was not caused by heating, but rather by inertial cavitation (Penny et al. 1993; Holland et al. 1996). Since 2000, we have published seven studies to evaluate whether inertial cavitation was responsible for ultrasound-induced lung hemorrhage (O'Brien et al. 2000, 2001a; Zachary et al. 2001b; O'Brien et al. 2002; Frizzell et al. 2003; O'Brien et al. 2003, 2004), and each study has lacked support for the hypothesis that inertial cavitation is the mechanism. The results of these studies also suggested that ultrasound-induced lung hemorrhage was likely related to the transfer of acoustic energy into lung tissue because more injury occurred in lung under deflated conditions (O'Brien et al. 2002; Oelze et al. 2003).

These findings led to a shift in established beliefs and resulted in the emergence of a hypothesis promoting the idea that ultrasound-induced lung hemorrhage was caused by mechanical phenomena other than inertial cavitation. Thus, the mechanical mechanism(s) capable

Address correspondence to: James F. Zachary, University of Illinois, 2001 South Lincoln Avenue, Urbana, IL 61802. E-mail: zacharyj@uiuc.edu

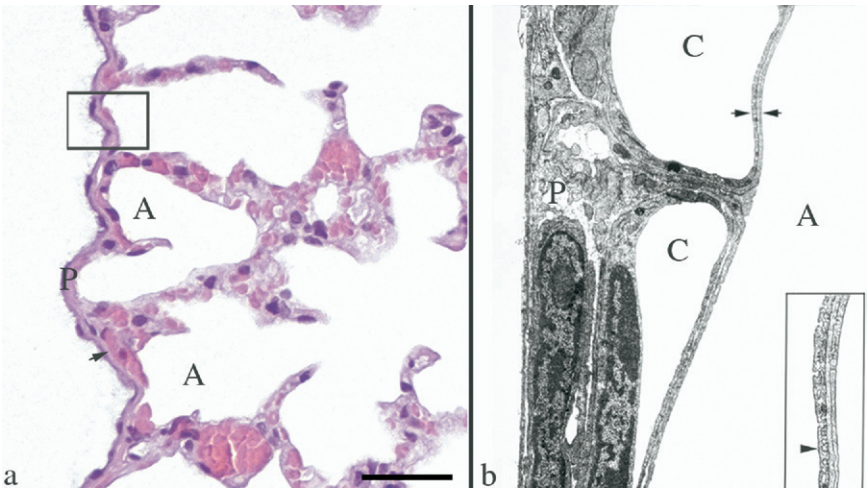

Fig. 1. Rat visceral pleura and the air–blood barrier. (a) The visceral pleural surface (P) of the rat lung is approximately 5 to 10 μm in thickness. It contains numerous capillaries (arrow), which separate it from the underlying air-filled alveolus (A). The box outlines the area of tissue demonstrated in Fig. 1b. Hematoxylin and eosin stain. Scale bar = 25 μm. (b) The illustration shows the area outlined by the box in Fig. 1a. The visceral pleural surface (P) of the rat lung is covered by a thin flat layer of mesothelial cells, is supported by fibrocytes and connective tissue and contains abundant capillaries (C). The air–blood barrier, formed by the endothelium of the capillary, basement membrane and type I pneumocytes (between the two arrows [this barrier varies in thickness, but has an arithmetic mean thickness of 1.25 μm, (Weibel and Knight (1964)]), is a point of impedance mismatch between the sound as it travels through tissue and fluids (blood) and abruptly hits the air in the alveolus (A). Inset: Higher magnification of the air–blood barrier (arrow head = endothelium). Transmission electron micrograph, lead citrate and uranyl acetate stain. Transmission electron micrograph courtesy of Dr. W. Haschek, Department of Pathobiology, University of Illinois.

of causing such damage are likely related to the stress that focused ultrasound imposes directly on the lung's air–blood barrier such as radiation forces (Chu and Apfel 1982; Elrod et al. 1989). We have shown that the histopathologic characteristics of the gross and microscopic lesions of pulsed ultrasound-induced lung hemorrhage are identical in four species (mice, rats, rabbits and pigs) (O'Brien et al. 2006) and that hemorrhage in these species occurs at exposure conditions similar to those used for scanning in human beings. Thus, these findings suggested a common pathogenesis in the initiation and propagation of the lesions at the gross and microscopic levels; however, the exact mechanism of injury remained elusive. Although we hypothesize that radiation forces are a plausible cause (and most difficult to prove) of ultrasound-induced lung hemorrhage (Fig. 1), the role of heating as the mechanism of injury needed to be reconsidered from a structural viewpoint because a gap remained in the experimental assessment of ultrasound-induced lung lesions. There has not been a histopathologic-based study that explicitly produced a heat-related lung lesion for comparison with an ultrasound-induced lung lesion.

Thus, the purpose of this study was to: (1) characterize the gross lesions in the lung of rats exposed to an infrared laser (a tissue heating source) and pulsed ultrasound (mechanical phenomena); (2) characterize the histopathologic lesions in the lung of rats exposed to an infrared laser and pulsed ultrasound and (3) compare the morphologic characteristics of the lesions in these groups with each other to provide further insight into the mechanism of ultrasound-induced lung hemorrhage.

MATERIALS AND METHODS

Animals

The experimental protocol was approved by the Institutional Animal Care and Use Committee (IACUC), University of Illinois, Urbana-Champaign, and satisfied all University and National Institutes of Health rules for the humane use of laboratory animals. Rats were selected as the experimental animal based on their use in our previous studies (O'Brien et al. 2000, 2001a, 2001b; Zachary et al. 2001a, 2001b; O'Brien et al. 2002; Frizzell et al. 2003; O'Brien et al. 2003; Oelze et al. 2003; O'Brien et al. 2004).

Five six-month-old Sprague Dawley rats (Harlan, Indianapolis, IN, USA) (271.6 $\pm$ 22.5 g) were anesthetized with ketamine hydrochloride (87.0 mg/kg) and xylazine (13.0 mg/kg), administered intraperitoneally. Anesthetized rats were placed in right lateral recumbency. Respiratory rates and peripheral vascular perfusion were monitored visually. Experiments were conducted in a room maintained at 22°C.

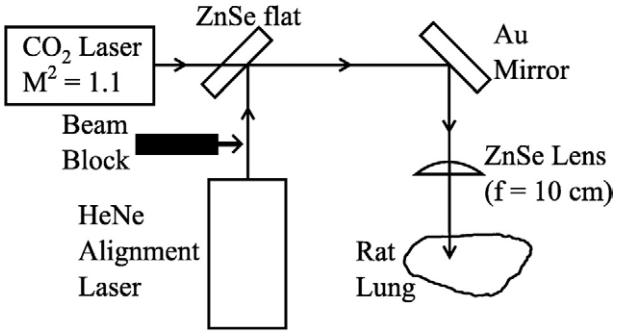

Fig. 2. Schematic diagram of the laser irradiation arrangement.

The skin over the left thoracic wall was exposed by removing hair with an electric clipper. A 12-mm vertical incision was made through the sixth intercostal space extending from the spinal column to the sternum. A rib spreader was used to open the incision to allow visualization and exposure of the lung to the laser beam. Although the lung was partially collapsed, the heart continued to beat and the lung was perfused with blood during the exposure period. A He-Ne laser was used to align the laser beam on the lung surface before exposure with the CO_2 laser. Three of the lungs were exposed for a duration of 25 s, one for 40 s and one for 10 s; all of the 600-mW CO_2 laser exposures yielded lesions.

After exposure and while under anesthesia (hearts still beating), rats were killed by cervical dislocation. The maximum time between incision and euthanasia was 120 s. The lungs were removed and examined grossly for the presence or absence of a lesion, digitally photographed and then fixed by immersion in 10% neutral-buffered formalin (pH 7.2) for a minimum of five days. After fixation, each lesion was bisected, embedded in paraffin, sectioned at 5 μm, mounted on glass slides, stained with hematoxylin and eosin and evaluated microscopically. The characteristics of these lesions were compared against lesions induced in lung by pulsed ultrasound. Lung lesions from previously published studies of ultrasound-induced lung hemorrhage in rats were pulled from the archives and served as the basis for comparison with laser-induced lung injury (O'Brien et al. 2001a, 2001b; Zachary et al. 2001a, 2001b).

Exposimetry

Infrared laser. A schematic diagram of the optical system employed for laser irradiation of rat lungs is shown in Fig. 2. A continuous-wave (CW) CO_2 laser ($\lambda \sim 10.6$ μm, $\hbar\omega \sim 0.12$ eV) (Model LASY-3; Access Laser Co., Marysville, WA, USA), having an output power of 600 mW and producing a near diffraction-limited beam (propagation factor of $M^2 = 1.1$) with a diameter (D) of 2.4 mm served as the infrared source. Throughout these experiments, the laser was operated in the lowest-order transverse mode (TEM_{00}), and the beam power was measured before and after each animal irradiation with a calibrated power detector (Model 210 laser power meter; Coherent, Inc., Santa Clara, CA, USA). The CO_2 laser beam was directed onto the rat lung by a flat gold mirror and focused by a ZnSe lens with a focal length (f) of 10 cm. At the focal point of the lens (the position of the rat lung surface), the CO_2 laser beam spot size (diameter $= 2w_0$) can be estimated by the relation (Silfvast 2004):

$$2w_0 = \frac{4M^2\lambda f}{\pi D} = 680\mu\text{m}. \quad (1)$$

Assuming a Gaussian beam profile, the expression for the laser irradiance (intensity) of the beam is given by:

$$E(r) = \frac{P}{\pi w_0^2/2}\, e^{-2r^2/w_0^2} \quad (2)$$

and the irradiance on the rat lung surface is given by:

$$E_0 = \frac{2P}{\pi w_0^2} = 330\ \text{W/cm}^2, \quad (3)$$

where P is the beam power measured at the terminus of the optical train, thereby accounting for losses introduced by the lens, mirror and ZnSe flat. Equations (1) and (2) were derived assuming the laser spot size to be given by $2w_0$, where w_0 is the radial position at which the azimuthally symmetric beam intensity has fallen to $e^{-2} \sim 13.5\%$ of its peak (on axis, $r = 0$) value.

A 5-mW He-Ne laser ($\lambda = 632.8$ nm) provided a visible beam to facilitate alignment of the optics, and the red and infrared laser beams were carefully overlapped and directed collinearly with a ZnSe flat. It must be emphasized that the He-Ne laser served solely to accurately position the CO_2 laser beam onto the desired portion of the rat lung. During the animal irradiation experiments, the red alignment beam was blocked, as indicated in Fig. 2.

A semi-infinite slab of tissue (lung) in air was the model used to estimate tissue temperature increase for which a Gaussian-shaped laser beam was assumed to be incident on the tissue surface. The time-dependent temperature increase ΔT as a function of axial distance z ($z = 0$ is the surface) and off-axis distance r is given by (van Gemert and Welch 1995)

$$\Delta T(z, r, t) = \frac{E_0\mu_a\tau}{\rho C}\cos\left(\frac{\pi\mu_a}{4}\right) J_0\left(\frac{2.4}{d/2}r\right)\left(1 - e^{-t/\tau}\right), \quad (4)$$

where the absorption coefficient μ_a at $\lambda \approx 10.6$ μm is estimated to be 50/mm, the density ρ is 414 kg/m^3

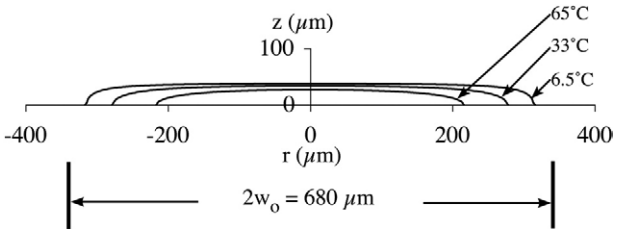

Fig. 3. Constant temperature increase profiles of the laser irradiation of 65, 33 and 6.5° C, assuming that the temperature increase at the origin is 130° C. The laser beam's diameter ($2w_o$) is 680 μm.

(O'Brien et al. 2002), the heat capacity C is 3.5 kJ/kg–°C and J_0 is the zeroth-order Bessel function. The time constant τ was estimated by two methods: (1) from the axial τ_z and radial τ_r time constants, $\tau^{-1} = \tau_z^{-1} + \tau_r^{-1} = \alpha\left\{\left(\frac{\pi\mu_a}{4}\right)^2 + \left(\frac{2.4}{d/2}\right)^2\right\}$, and (2) from the penetration depth δ (= 20 μm) of laser light into tissue, $\tau = \delta^2/4\alpha$, where the thermal diffusion time α is 0.26 mm^2/s. Thus, respectively, the time constants are 0.38 and 2.4 ms. For an approximate time constant of 1 ms, the on-axis (r = 0) temperature increase at the surface (z = 0) for t $\gg$ 1 ms is 130° C. The off-axis temperature increase, $J_0(7.1r)$, where r is in mm, decreases to one half the on-axis value at 210 μm, and the on-axis temperature increase, Cos (39 z), where z is in mm, decreases to one half the surface value at 27 μm (Fig. 3). Thus, it is possible that, on-axis at the surface, tissue ablation occurred, but a short distance from this location, significant nonablative thermal damage resulted.

Ultrasound

During the last eight y, our laboratories have evaluated and characterized macroscopically and microscopically ultrasound-induced lung hemorrhage in mice, rats, rabbits and pigs over a wide range of animal weights (mouse 22 to 32 g; rat 190 to 330 g; rabbit 1.9 to 2.9 kg and pig 1 to 25 kg) using *in situ* peak rarefactional pressures ranging between 0.3 (shams) and 17 MPa (MI = 5.7). In addition, there are significant interspecies structural differences of the lungs, even when lungs and associated structures are evaluated at a subgross level (Plopper and Pinkerton 1992). Ultrasound-induced lung lesions were similar in all species, under all exposure conditions. Ultrasound exposure conditions and transducer calibration procedures used in these studies were described previously (Sempsrott and O'Brien 1999; Sempsrott 2000; O'Brien et al. 2001a, 2001b; Zachary et al. 2001a, 2001b) and based on established standards (AIUM/NEMA 1998; ODS 1998).

Pathologic evaluation

Grossly and microscopically, each lung exposed to infrared laser was evaluated and described based on the characteristics of the lesions in a manner similar to those used in previous studies of ultrasound-induced lung hemorrhage (Zachary et al. 2001a, 2001b). Microscopically, each lesion was evaluated for changes affecting the visceral pleura, microvasculature, alveolar septa and other lung microanatomy (Zachary et al. 2001a, 2001b).

RESULTS

Pathologic evaluation

A comparison of the lesions induced by pulsed ultrasound and infrared laser energy in rat lung is shown in Fig. 4.

Gross lesions

Grossly, lesions induced in the lung by pulsed ultrasound were consistent with hemorrhage. Hemorrhage occurred under the visceral pleural, was oval and red to dark-red (Fig. 4a). No hemorrhage was detected on the pleural surface and suggested that the "barrier" integrity of the visceral pleura was intact. Hemorrhage extended into subjacent lung, forming a "cone" of varied depths, whose base was at the visceral pleural surface. The pleural surface overlying the lesion was often raised above the normal contour because of hemorrhage filling and enlarging alveoli. Such lesions were identical in mice, rats, rabbits and pigs.

Lesions induced in the lung by infrared laser were consistent with thermal coagulation as the cause of necrosis. Necrosis occurred through and under the visceral pleural, was oval and dark-red to brown (Fig. 4b). It was detected on the pleural surface (irregular depressed cavity in the center of the lesion) (Fig. 4b) and this suggested that the "barrier" integrity of the visceral pleura was broken. Necrosis extended into subjacent lung, forming a "cone" of varied depths, whose base was at the visceral pleural surface. The pleural surface overlying the lesion at the outer margins of the lesion was often raised above the normal contour (Fig. 4b); however, the central area of the lesion formed a necrotic cavity of varied depth.

Microscopic lesions

Microscopically at a low magnification, lesions induced in the lung by both pulsed ultrasound and infrared laser formed a conical pattern (Figs. 4c, d). The contour of the visceral pleura was raised in lung exposed to ultrasound when compared with the depressed surface of the lung exposed to laser energy (necrosis). This depression was the result of tissue collapse, coagulation and loss attributable to necrosis; however, at the outermost margins of this cone of

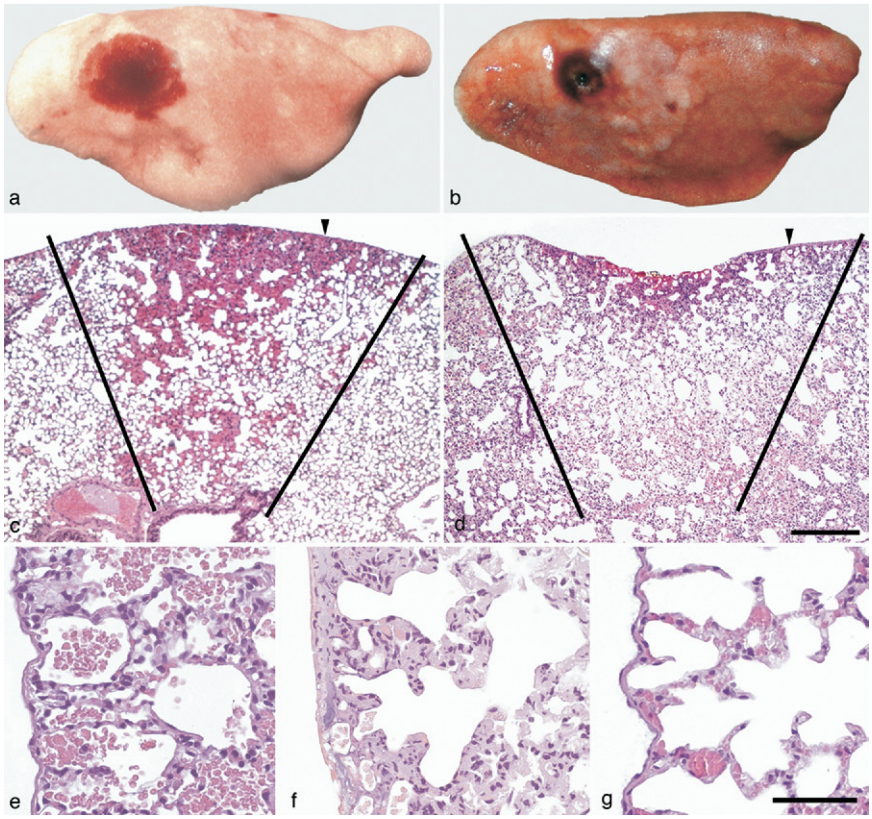

Fig. 4. Ultrasound- and laser energy-induced lesions in rat lung. Gross lessons: (a) Ultrasound-induced lesions were consistent with hemorrhage, occurred under the visceral pleural and were oval and red to dark-red. (b) Laser energy-induced lesions were consistent with necrosis. Necrosis occurred through and under the visceral pleural, was oval and dark-red to brown. The pleural surface was injured as shown by the irregular depressed cavity in the center of the lesion. Microscopic (subgross) lesions: (c) With ultrasound, the lesion formed a "cone" of varied depths (see black lines), whose base was at the visceral pleural surface, the pleural surface was intact and elevated (hemorrhage) and the underlying alveoli were filled with hemorrhage (arrowhead = sample point for Fig. 4e). (d) With laser energy, the lesion also formed a "cone" of varied depths (see black lines) whose base was at the visceral pleural surface, the pleural surface was depressed and damaged (necrosis) and the underlying alveoli were coagulated (necrosis) (arrowhead = sample point for Fig. 4f). Microscopic lesions: (e) With ultrasound, lung had no visible lesions other than alveolar hemorrhage; (f) With laser energy, the pleura and septa were necrotic with coagulation of proteins (acute coagulative necrosis) and nucleic acid (nuclear pyknosis); and (g) Normal rat pleura and subjacent alveoli. Hematoxylin and eosin stain. Scale bar = 200 μm for Fig. 2c, d. Scale bar = 50 μm for Fig. 2e-g.

necrosis, the microvasculature was filled with blood in a response (active hyperemia) to injury. At a higher magnification, lung exposed to ultrasound had no visible lesions other than hemorrhage into alveoli (Fig. 4e), whereas lung exposed to infrared laser had lesions consistent with thermal coagulation (necrosis) (Fig. 4f, g [control]). These latter lesions included coagulation of proteins (acute coagulative necrosis) and nucleic acid (nuclear pyknosis) in tissue layers and cells, including erythrocytes, forming or occupying the visceral pleura, alveolar septa, microvasculature and other lung structures (Figs. 4f and 5a, b). Microscopic lesions induced by pulsed ultrasound in the lung of mice, rats, rabbits and pigs in our studies were identical.

DISCUSSION AND SUMMARY

In this study, we have provided additional evidence to support the findings of Hartman et al. (1992), that ultrasound-induced lung hemorrhage is not attributable to a thermal mechanism. This support is based on two facts derived from this study: (1) injury to lung induced by infrared laser had a cytomorphologic pattern characteristic of heat induced (thermal) injury of biologic tissues and (2) injury to lung induced by pulsed ultrasound (in mice, rats, rabbits and pigs) did not show any cytomorphologic parallel when compared with injury induced by infrared laser.

A nonthermal mechanism for ultrasound-induced lung hemorrhage is also supported by the work of Penny

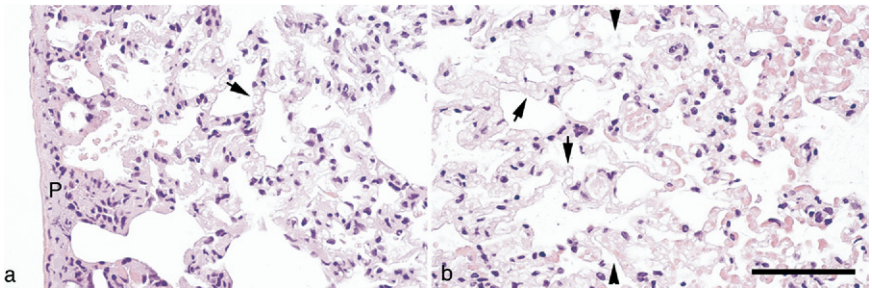

Fig. 5. Laser energy-induced lesions in rat lung. (a) The pleura is homogeneous and light pink (tissue stains poorly with hematoxylin and eosin [H&E] stain) with retention of tissue architecture (necrosis). It also contains dead cells with clumped chromatin (nuclear pyknosis). This histopathologic appearance is also present in alveolar septa and there is some cellular debris in alveoli. Red blood cells in capillaries under the pleura and in alveolar septa are necrotic and their remnants form clear oval spaces (arrow). (b) At the margins of the necrotic tissue (conical shape) deep within the lung are intact (living) alveolar septa (tissue to the right of the line formed by the arrowheads) that contain abundant erythrocytes (active hyperemia). Alveolar septa with their red blood cells (arrows) are necrotic (tissue to the left of the line formed by the arrow-heads). H&E stain. Scale bar = 50 μm.

et al. (1993), in which they: (1) reported using transmission electron microscopy, disruption of alveolar septa (epithelial cells [type 1 pneumocytes], endothelial cells and basal laminae), resulting in alveolar hemorrhage and (2) did not describe ultrastructural lesions in lung consistent with a thermal mechanism of injury. They attributed the septal lesions to a "lytic cell death" mechanism, possibly cavitation resulting in cell membrane disruption. Our recent studies do not support inertial cavitation as a mechanism for ultrasound-induced lung hemorrhage (O'Brien et al. 2000, 2001a; Zachary et al. 2001b; O'Brien et al. 2002; Frizzell et al. 2003; O'Brien et al. 2003, 2004).

A rat lung inflation study of ultrasound-induced lung hemorrhage showed that the occurrence of hemorrhage in rats was directly correlated to the level of lung inflation, with greater hemorrhage at deflation (O'Brien et al. 2002). A follow-up study showed that the impedance of the rat lungs at deflation was closer to the characteristic impedance value of water than for the inflated cases (Oelze et al. 2003), suggesting that more ultrasonic energy was transferred into deflated lungs than into the inflated lungs. These experimental observations led us to suggest that lung temperature increase from ultrasound might be a plausible cause for lung hemorrhage. Our typical 10-s exposure duration 1-kHz pulse repetition frequency ultrasound-induced lesion thresholds were in the approximate range of peak rarefactional pressures between 2 and 4 MPa for center frequencies between 3 and 6 MHz. These values yielded measured spatial-peak, pulse-average intensities approximately between 100 and 600 W/cm^2, and spatial-peak, temporal-average intensities between 0.1 and 0.6 W/cm^2 (typical pulse durations were $\sim$1 μs). The initial time rate of change of temperature is given by Fry and Fry (1953):

$$\frac{\Delta T}{\Delta t} = \frac{2\alpha I_{TA}}{C_h} \quad (5)$$

and it is assumed that no heat is lost by conduction, convection or any other heat removal processes. The attenuation coefficient for fresh collapsed canine lung between 2.4 and 7.4 MHz was measured to be 10 dB/cm-MHz (Bauld and Schwan 1974), and between 1 and 5 MHz for noncollapsed lung was measured to be 16 dB/cm-MHz (Dunn 1974). Using the higher attenuation coefficient (and assuming that it is an absorption coefficient α), and assuming the lung's specific heat can be approximated by water (C_h = 4.18 J/cm^3–°C), the initial time rate of change of temperature is calculated to be 1.6 and 3.2°C/s for a temporal-average intensity I_{TA} of 0.6 W/cm^2. This calculation is valid only for short exposure times; for longer exposure times, heat removal processes become significant. Nevertheless, for the first couple of seconds, there would be minimal heat removal, suggesting that the lung temperature might increase to a level that could cause damage (possibly hemorrhage) *via* a thermal mechanism.

However, based on the Hartman et al. (1992) findings, a temperature increase less than 1°C should result because our exposure durations were only 10 s, whereas Hartman et al. (1992) used a 300-s exposure duration to yield a steady-state temperature increase. Also, our –6-dB beam widths were typically in the range of 500 to 600 μm, whereas that for Hartman et al. (1992) was 3.9 mm.

Because the experimental evidence suggests that a thermal mechanism may not be involved in ultrasound-induced lung hemorrhage, it has not been definitively ruled out. The character of the septal injury described by Penny et al. (1993) could result from thermal injury if it

occurred on a structural scale (nm or Å scale) not detectable using transmission electron microscopy. Second, if inertial cavitation were involved at this scale, then both mechanical and thermal phenomena would need to be considered in developing a hypothetical mechanism of injury. Shear stress (AIUM 2000b; Church et al. 2006; Miller et al. 2006) or heat and microjets arising from inertial cavitation (AIUM 2000b; Church et al. 2006; Dalecki 2004) are the most likely physical forms of injury that could produce damage not detectable using transmission electron microscopy. Also, because lung is not typical of other soft tissues, and if inertial cavitation is indeed the responsible damage mechanism (although our experimental findings do not support this hypothesis), then it might be feasible to hypothesize that the enhanced heating reported when ultrasound interacts with ultrasound contrast agents (Holt and Roy 2001; Sokka et al. 2003; Razansky et al. 2006) is likewise applicable in the lung.

Based on the results of all studies that have examined ultrasound-induced lung hemorrhage, radiation force (mechanical phenomena) acting at the air–blood barrier is hypothesized to be a likely mechanism for this lesion (Fig. 1). The following concept is similar to a focused ultrasound beam that is incident from water onto a water-air boundary (Fig. 6). The air-blood barrier is approximately 100 nm in thickness and represents an area of abrupt impedance mismatch between tissue and air in the alveolus. We hypothesize that, when sound travels through tissue and hits this area of impedance mismatch, it is reflected off the air–blood barrier. The pulse repetition frequency of the reflected sound results in a pulsed and rapid deformation and rebound of the air–blood barrier and, with time, the cell membranes of this layer fracture from shear stress caused by repetitive motion. This radiation force literally "punches" a hole in the air–blood barrier of sufficient size (~5 to 7 μm) to allow blood plasma and erythrocytes to escape into the alveolus (lung hemorrhage) before the break is repaired by the coagulation cascade (Mitchell 2005). The initial impedance mismatch occurs at the visceral pleura at the air–blood barrier that separates the pleura from the underlying alveolus (Fig. 1). With disruption of this air–blood barrier, alveolar hemorrhage ensues and the acoustic energy easily spreads through the hemorrhage to the next air–blood barrier of an intact and air-filled alveolus (Fig. 1). This process occurs repeatedly until the gross and microscopic lesions, characteristic of ultrasound-induced lung hemorrhage (described above), develop in the lung.

The results from this study are another step in developing a better understanding of the pathogenesis of ultrasound-induced lung hemorrhage and the mechanisms of tissue injury that occurs; however, the hypothesis developed here will be a difficult biologic challenge to prove at the structural and/or functional levels.

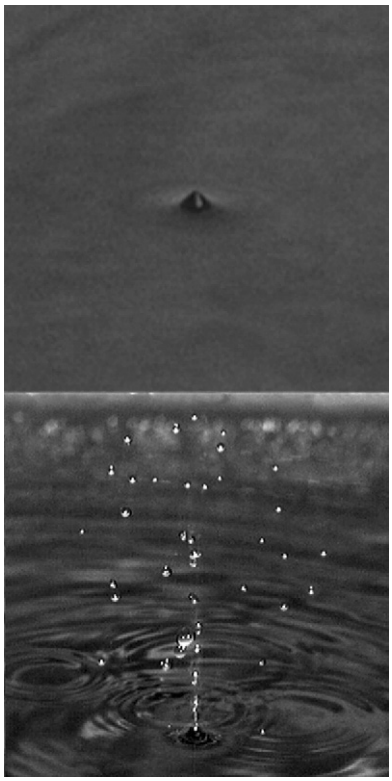

Fig. 6. A simplified *in vitro* model for the region near the lung pleural surface is a water–air interface. The 6-cm diameter 3.32-MHz f/2.25 focused ultrasound source has a free-field pulse-echo −6-dB beam width at the focus of 6.7 mm. The focus is at the water–air interface. The free-field *in vitro* peak rarefactional pressures at the focus are 1.4 (top) and 1.8 (bottom) MPa. Their respective temporal-average intensities at the focus are 1.1 and 1.8 W/cm^2. The pulse duration is 12.4 μs and the pulse repetition frequency is 1 kHz.

Acknowledgements—We thank the Bioacoustics Research Laboratory, the Laboratory for Optical Physics and Engineering, and the staff of the Histopathology Laboratory, College of Veterinary Medicine, University of Illinois, for technical contributions. This study was supported, in part, by NIH grant R37EB02641 (formerly HL58218) awarded to WDO and JFZ.

REFERENCES

AIUM. Mechanical Bioeffects from Diagnostic Ultrasound: AIUM Consensus Statements, Section 4—bioeffects in tissues with gas bodies. American Institute of Ultrasound in Medicine [review]. J Ultrasound Med 2000a Feb;19(2):97–108:154–168, 2000a.

AIUM. Mechanical Bioeffects from Diagnostic Ultrasound: AIUM Consensus Statements, Section 6—Mechanical bioeffects in the presence of gas-carrier ultrasound contrast agents. American Institute of Ultrasound in Medicine [review]. J Ultrasound Med 2000b Feb;19(2):120–142:154–168, 2000b.

AIUM. Mechanical Bioeffects from Diagnostic Ultrasound: AIUM Consensus Statements, Section 7—discussion of the mechanical index and other exposure parameters. American Institute of Ultra-

sound in Medicine [review]. J Ultrasound Med 2000c Feb;19(2):143–148:154–168, 2000c.
AIUM/NEMA. Acoustic Output Measurement Standard for Diagnostic Ultrasound Equipment, American Institute of Ultrasound in Medicine, Laurel, MD and National Electrical Manufacturers Association, Rosslyn, VA, 1998.
Bauld TJ, Schwan HP. Attenuation and reflection of ultrasound in canine lung tissue. J Acoust Soc Am 1974;56(5):1630–1637.
Chu B-T, Apfel RE. Acoustic radiation pressure produced by a beam of sound. J Acoust Soc Am 1982;72(6):1673–1687.
Church CC, Carstensen EL, Nyborg WL, Carson PL, Frizzell LA, Bailey MR. The risk of exposure to diagnostic ultrasound in postnatal subjects—Nonthermal mechanisms. J Ultrasound Med 2007; in press.
Dalecki D. Mechanical bioeffects of ultrasound. Annu Rev Biomed Eng 2004;6:229–248.
Dunn F. Attenuation and speed of ultrasound in lung. J Acoust Soc Am 1974;56(5):1638–1639.
Elrod SA, Hadimioglu B, Khuri-Yakub BT, et al. Nozzleless droplet formation with focused acoustic beams. J Appl Phys 1989;56(9): 3441–3447.
Frizzell LA, Zachary JF, O'Brien WD Jr. Effect of pulse polarity and energy on ultrasound-induced lung hemorrhage in adult rats. J Acoust Soc Am 2003;113(5):2912–2918.
Fry WJ, Fry RB. Temperature changes produced in tissue during ultrasound irradiation. J Acoust Soc Am 1953;25(1):6–11.
Hartman CL, Child SZ, Penney DP, Carstensen EL. Ultrasonic heating of lung tissue. J Acoust Soc Am 1992;91(1):513–516.
Holt RG, Roy RA. Measurements of bubble-enhanced heating from focused, MHz-frequency ultrasound in a tissue-mimicking material. Ultrasound Med Biol 2001;27(10):1399–1412
Holland CK, Deng CX, Apfel RE, Alderman JL, Fernandez LA, Taylor KJ. Direct evidence of cavitation in vivo from diagnostic ultrasound. Ultrasound Med Biol 1996;22(7):917–925.
Miller DL, Averkiou MA, Brayman AA, et al. Bioeffects considerations for diagnostic ultrasound contrast agents. J Ultrasound Med 2007; in press.
Mitchell RN. Hemodynamic disorders, thromboembolic disease, and shock. In Kumar V, Abba AK, Fausto N (eds): Robbins and Cotran Pathologic Basis of Disease, 7th ed. Philadelphia: W.B Saunders; 2005:119–134.
O'Brien WD Jr, Frizzell LA, Weigel RM, Zachary JF. Ultrasound-induced lung hemorrhage is not caused by inertial cavitation. J Acoust Soc Am 2000;108(3 Pt 1):1290–1297.
O'Brien WD Jr, Kramer JM, Waldrop TG, et al. Ultrasound-induced lung hemorrhage: Role of acoustic boundary conditions at the pleural surface. J Acoust Soc Am 2002;111(2):1102–1109.
O'Brien WD Jr, Frizzell LA, Schaeffer DJ, Zachary JF. Superthreshold behavior of ultrasound-induced lung hemorrhage in adult mice and rats: Role of pulse repetition frequency and pulse duration. Ultrasound Med Biol 2001a;27(2):267–277.
O'Brien WD Jr, Simpson DG, Frizzell LA, Zachary JF. Effect of contrast agent on the incidence and magnitude of ultrasound-induced lung hemorrhage in rats. Echocardiography 2004;21(5):417–422.
O'Brien WD Jr, Simpson DG, Frizzell LA, Zachary JF. Superthreshold behavior and threshold estimates of ultrasound-induced lung hemorrhage in adult rats: Role of beamwidth. IEEE Trans Ultrason Ferroelectr Freq Control 2001b;48(6):1695–1705.
O'Brien WD Jr, Simpson DG, Frizzell LA, Zachary JF. Threshold estimates and superthreshold behavior of ultrasound-induced lung hemorrhage in adult rats: role of pulse duration. Ultrasound Med Biol 2003;29(11):1625–1634.
O'Brien WD Jr, Yan Y, Simpson DG, et al. Threshold estimation of ultrasound-induced lung hemorrhage in adult rabbits, and comparison of thresholds in mice, rats, rabbits and pigs. Ultrasound Med Biol 2006;32:1793–1804.
ODS. Standard for the Real-Time Display of Thermal and Mechanical Acoustic Output Indices on Diagnostic Ultrasound Equipment, Rev 1, American Institute of Ultrasound in Medicine, Laurel, MD and National Electrical Manufacturers Association, Rosslyn, VA, 1998.
Oelze ML, Miller RJ, Blue JP Jr, Zachary JF, O'Brien WD Jr. Impedance measurements of ex vivo rat lung at different volumes of inflation. J Acoust Soc Am 2003;114(6 Pt 1):3384–3393.
Penney DP, Schenk EA, Maltby K, Hartman-Raeman C, Child SZ, Carstensen EL. Morphological effects of pulsed ultrasound in the lung. Ultrasound Med Biol 1993;19(2):127–135.
Plopper CG, Pinkerton KE. Structural and cellular diversity of the mammalian respiratory system. In Parent RA (ed): Comparative Biology of the Normal Lung. Boca Raton, FL: CRC Press; 1992: 1–5.
Razansky D, Einziger PD, Adam DR. Enhanced heat deposition using ultrasound contrast agent—Modeling and experimental observations. IEEE Trans Ultrason Ferroelectr Freq Control 2006;53(1): 137–147.
Sempsrott JM. Experimental evaluation of acoustic saturation [Master's Thesis]. Department of Electrical and Computer Engineering, University of Illinois, Urbana, IL 2000.
Sempsrott JM, O'Brien WD Jr. Experimental verification of acoustic saturation. Proceedings of the 1999 IEEE Ultrasonics Symposium, 1999:1287–1290.
Silfvast WT. Chapter 12. Stable laser resonators and Gaussian beams. In: Laser Fundamentals, 2nd ed. Cambridge, UK: Cambridge University Press; 2004.
Sokka SD, King R, Hynynen K. MRI-guided gas bubble enhanced ultrasound heating in in vivo rabbit thigh. Phys Med Biol 2003; 48(2):223–241.
van Gemert MJC, Welch AJ. Approximate solutions for heat conduction: Time constants. In Welch A, van Gemert MJC (eds): Optical-Thermal Response of Laser-Irradiated Tissue. New York: Plenum Press; 1995:411–443.
Weibel ER, Knight BW. A morphometric study on the thickness of the pulmonary air-blood barrier. J Cell Biol 1964;21:367–396.
Zachary JF, Frizzell LA, Norrell KS, Blue JP, Miller RJ, O'Brien WD Jr. Temporal and spatial evaluation of lesion reparative responses following superthreshold exposure of rat lung to pulsed ultrasound. Ultrasound Med Biol 2001a;27(6):829–839.
Zachary JF, Sempsrott JM, Frizzell LA, Simpson DG, O'Brien WD Jr. Superthreshold behavior and threshold estimation of ultrasound-induced lung hemorrhage in adult mice and rats. IEEE Trans Ultrason Ferroelectr Freq Control 2001b;48(2):581–592.